# Crystal polymorphism in pendimethalin herbicide is driven by electronic delocalization and changes in intramolecular hydrogen bonding. A crystallographic, spectroscopic and computational study

**Gerald W. Stockton,*[a] Russell Godfrey,[b] Peter Hitchcock,[c] Richard Mendelsohn,[d] Patrick C. Mowery,[a] Srinivasan Rajan[a] and Anthony F. Walker[e]**

[a] *American Cyanamid Company, Agricultural Products Research Division, PO Box 400, Princeton, New Jersey 08543 0400, USA*
[b] *Wyeth Ayerst Research, Pharmaceutical Sciences, 154 Fareham Road, Gosport, Hants, UK PO13 0AS*
[c] *School of Molecular Sciences, Sussex University, Sussex, UK BN1 9QJ*
[d] *Department of Chemistry, Rutgers University, Newark, New Jersey 07102, USA*
[e] *Cyanamid Agriculture Ltd, 154 Fareham Road, Gosport, Hants, UK P013 0AS*

**Pendimethalin, *N*-(1-ethylpropyl)-3,4-dimethyl-2,6-dinitrobenzenamine, is a potent herbicide that exists in two differently coloured polymorphic crystal habits. Triclinic pendimethalin I ($P\bar{1}$) is the orange-coloured thermodynamically stable form, whereas monoclinic pendimethalin II ($P2_1/c$) is a bright-yellow metastable form. The latter is normally produced first upon cooling the molten chemical, whereas the orange form is formed by a polymorphic phase transition which occurs slowly upon long term storage of the yellow form at temperatures below its melting point. Such phase transitions are rapidly revealed by calorimetry. The crystal structures of the polymorphs have been determined using single crystal X-ray diffraction. Solid state NMR spectroscopy, vibrational spectroscopy and UV–VIS spectroscopy were applied to further study the nature of the polymorphism in terms of intra- and inter-molecular properties. Solid state CP-MAS $^{13}C$ NMR spectroscopy was shown to be the method of choice for quantitative analysis of polymorphic mixtures. The differences in spectral properties and crystal habits were investigated by computational methods which included molecular exciton, molecular orbital and molecular mechanics calculations. The dramatic colour change from yellow to orange-red during the polymorphic transition is discussed in terms of competing inter- and intra-molecular electronic effects. The driving force for the yellow (II) to orange (I) polymorphic transition is attributed to the change in the electronic delocalization achieved from shortening, strengthening, and partially straightening the 'bent' hydrogen bond between the secondary amino hydrogen and an oxygen of the 6′-nitro group. This results in increased overlap between the amino nitrogen's lone pair and the π-electron orbitals of the aromatic ring. The calculated lattice stabilization energy due to this process is 4 to 5 kcal mol$^{-1}$, and the relative lattice energies are consistent with the observed stabilities of the polymorphs. The slow kinetics of the polymorphic transition are largely governed by the steric interaction of the 1-ethylpropyl side chain and the two nitro groups. During crystallization, the more compact side chain conformation required to form the energetically more stable orange (I) polymorph appears to be more difficult to achieve than that required for the yellow (II) polymorph.**

## Introduction

Polymorphism in crystals of both organic and inorganic compounds, and control of crystal habit and crystal growth are topics of renewed scientific and commercial interest.[1,2] Methods for the detection and characterization of organic polymorphs have been recently reviewed.[3] The size and shape of organic crystals are important parameters that must be controlled in industrial crystallization processes. For example, dissimilar crystal habits of drug molecules exhibit different solubilities and dissolution rates which usually affect biological efficacy and safety. In consequence, the rational design of chemical additives for the control of crystal habit and/or crystal growth has recently become an active and intriguing area of molecular modeling research.[4–9] This has also stimulated a search for new methods for the *ab initio* prediction of polymorphism,[1,10,11] and for predicting the relationship between the structure of the crystallographic unit cell and the shape of the macroscopic crystal.[12–17] The prediction of crystal structure by calculation must first successfully identify the most thermodynamically stable (low energy) polymorphs at a given temperature, as well as modeling nucleation kinetics to predict which polymorph will crystallize first.[18–21]

The notion that detailed computational methods can be used to infer an understanding of the structural effects underlying polymorphism has stimulated the current work, in which we have applied a variety of experimental and computational methods to study the polymorphism of a compound of interest.

Pendimethalin [*N*-(1-ethylpropyl)-3,4-dimethyl-2,6-dinitrobenzenamine, *cf.* Fig. 1], is an important broad spectrum herbicide for pre-emergence and early post-emergence control of most grassy weeds and many broad leaf weeds in cereals, fruits, vegetables and turf.[22,23] Pendimethalin, like other dinitroaniline herbicides, interferes with polymerization of the microfilament protein tubulin, inhibiting cell division in plants.[24]

In the solid state, pendimethalin exhibits two crystal habits of dramatically different colours. A thermodynamically stable bright orange form, pendimethalin I, melts upon heating and recrystallizes to produce pendimethalin II, a bright yellow form which melts at a higher temperature. When liquid pendimethalin

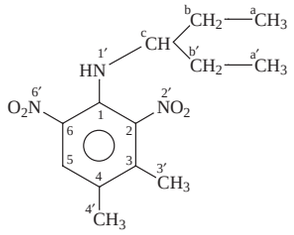

**Fig. 1** Pendimethalin herbicide with the numbering scheme used in the assignment of NMR spectra

is cooled from temperatures above its melting point, yellow crystals are formed which, upon cooling further to room temperature, are thermodynamically metastable with respect to the orange form. Under thermodynamic control, the solid yellow polymorph slowly converts to a more stable orange form, a process which can take months or years to complete at 25 °C. Also, these two crystal habits can be made selectively by recrystallizing pendimethalin from an appropriate solvent.

The slow transition from the yellow to the orange form of pendimethalin and its concomitant change in physical properties presents a significant problem in manufacturing stable formulations of the herbicide for commercial use. Herbicides are commonly formulated for their end use application as liquid concentrates, emulsions or dispersible solids. Some such formulations contain micronized crystals of the active ingredient in an aqueous suspension stabilized by surfactants.[25] Solid formulations are made by adsorbing the active ingredient on a porous inorganic excipient such as silica, alumina or clay, which are made 'wettable' by the addition of surfactants. Such concentrated formulations are dispersed (highly diluted) in water, immediately before use, and then sprayed on the field or crop. Solid-in-liquid dispersions are stable within a narrow range of particle size. Thus, elimination of the crystal growth which accompanies the yellow (II) to orange (I) transition is a significant factor in creating a stable formulated product suitable for agricultural use.[26]

In this report, we have attempted to characterize the crystallographic, spectroscopic and thermodynamic properties of pendimethalin, both experimentally and by theoretical calculations. The latter are of interest due to the relatively sparse literature on molecular modeling applications in condensed phases, and for rationalizing the experimental results. These results were extremely valuable in understanding the nature of crystal polymorphism in pendimethalin and they provided a basis for the discovery of stable formulations of this important herbicide. The utility of the various methods as analytical tools for quantifying polymorphic mixtures is also discussed.

## Experimental

### Materials

A sample of analytical standard grade (ASG) orange pendimethalin I (purity = 99.5%) was provided by American Cyanamid Company. A sample of the yellow form, pendimethalin II, suitable for spectroscopy and calorimetry was obtained by dissolving a sub-sample of the orange form in methanol at 50 °C, pouring the solution into cold water, and separating and drying the yellow solid.

Large single crystals suitable for X-ray diffraction studies were prepared as follows: Sixty grams (60 g) of ASG pendimethalin was dissolved in 110 ml of methanol at 60 °C and kept at this temperature for 15 min. The solution was cooled slowly while continuously seeding with the small crystals of yellow pendimethalin (prepared as above), or with orange pendimethalin, until crystallization occurred. The large crystals of orange or yellow pendimethalin were separated, washed quickly with methanol, and air dried. The most suitable single crystals were hand picked.

### Differential scanning calorimetry

Calorimetric melting profiles were obtained on a Setaram DSC III differential scanning calorimeter, with a scan rate of 1 °C $min^{-1}$.

### X-Ray diffraction

Single crystal X-ray diffraction patterns were collected on an Enraf Nonius CAD4 diffractometer in the $\theta$–$2\theta$ mode with Mo-K$\alpha$ radiation ($\lambda = 0.710\,69$ Å) and a graphite monochromator. The structures were solved using the MULTAN computer program.[27]

### Nuclear magnetic resonance

Cross polarization magic angle spinning (CP-MAS) $^{13}C$ spectra of the polymorphs were obtained on a Bruker CXP 300 NMR spectrometer. Most experiments used an Andrew type rotor,[28] although those involving solid/liquid suspensions used a Schneider[29] type sealed barrel rotor. The NMR pulse sequence TOSS[30] was used to suppress spinning side bands in MAS spectra. Similarly, $^{15}N$ spectra were obtained on a Bruker MSL 300 spectrometer. All $^{13}C$ chemical shifts, $\delta$, are reported relative to tetramethylsilane (TMS) at 0 ppm. For solution spectra, the $^{13}C$ chemical shifts were measured relative to internal TMS, whereas in CP-MAS spectra of solids, the shifts were measured relative to an external reference: the carbonyl resonance of solid glycine at 176.07 ppm *vs.* TMS. The $^{15}N$ spectra were referenced to the $^{15}NO_3$ resonance of ammonium nitrate, defined as 0 ppm. The solid state proton NMR spectra were recorded on a Bruker CXP 200 NMR spectrometer using the combined rotation and magic angle spinning (CRAMPS) technique.[31] An MREV 8 pulse sequence with a cycle time of 48 μs was used, sampling twice per cycle and applying a scaling factor of 2. Hence, the effective sampling rate was 12 μs, yielding a spectral width of 80 kHz.

### Raman spectroscopy

Resonance Raman spectra were obtained using a Jarrell Ash 3/4 meter double monochromator equipped with an argon ion laser, providing 5145 Å (green) excitation, and a photon counting detector. The sample holder was a rotating cell[32] onto which a thin layer of potassium bromide was deposited. The pendimethalin powder was pressed onto the KBr surface using pressures ranging between 6000 and 20 000 psi (it is noteworthy that application of high pressures briefly to the yellow form did not cause conversion to the orange polymorph). Most scans were made in the region 1200–1400 $cm^{-1}$, since no significant bands were found outside this region. Several scans were averaged in a computer to improve the signal to noise ratio.

### Infrared spectroscopy

Samples for infrared analysis were prepared by dispersing pendimethalin I or II at a level of *ca.* 1.5% in potassium bromide. Diffuse reflectance Fourier transform infrared spectra (DRIFTS) were recorded on Bomem model MB 120 and Bio-Rad FTS 60A spectrometers equipped with room temperature DRIFTS accessories.

### UV–VIS spectroscopy

UV–VIS spectra of pendimethalin were measured in hexane solution and in the solid state. Solid samples were prepared by grinding pendimethalin (0.5 mg) with potassium bromide (200 mg). The UV–VIS spectra were recorded on a Perkin-Elmer Lambda IV spectrometer. Solutions were examined in 1 cm and 1 mm cells, while the spectra of solid samples were obtained using an integrating sphere detector purchased from Labsphere Inc.

### Molecular modeling

Molecular modeling was carried out with the aid of SYBYL

molecular modeling software[33] installed on a Silicon Graphics Iris Crimson computer system equipped with quad R6000 processors, and also the CERIUS crystal modeling software[34] installed on a Silicon Graphics Iris Indigo Elan computer with a single R4000 processor.

Two different approaches were used to refine the X-ray coordinates for subsequent lattice energy and molecular orbital calculations. In the first approach, using SYBYL, the geometry of a single molecule was optimized within the crystal field of the neighboring molecules. The unit cells were constructed and replicated in three dimensions. The energy of a central molecule was calculated as a function of the non bonded cutoff and interactions at distances greater than 15 Å were found to be negligible. Molecules that exceeded the 15 Å limit were selectively deleted to keep the total atom count within manageable bounds. Thus, the lattice was approximately spherical. All of the molecules except the central molecule were defined as an 'aggregate' with fixed atomic coordinates. Then, the atomic coordinates of the central molecule were optimized by energy minimization using the method of steepest descent, which avoids a major departure from the X-ray structure. Gasteiger Hückel charges and the Tripos force field were used with a non bonded cutoff of 15 Å.

The optimized central molecule was then used to build a new unit cell of the same cell dimensions, but with slightly different atomic coordinates. The unit cell again was replicated into a 15 Å radius, approximately spherical lattice, and the entire process of optimizing the central molecule in the force field of the aggregate was repeated. Although this process could have been continued until a steady state was reached, the process was terminated after the third cycle due to the long computation time involved. The resulting energies were used to calculate the lattice energy, as discussed in the following Section, and the refined structures were used in subsequent molecular orbital calculations.

In the second approach, the CERIUS software was used, beginning with the X-ray coordinates, to build a unit cell, then an extended lattice, and the entire lattice was optimized under periodic boundary conditions. Note that CERIUS uses the Dreiding force field.[35] As in the first method, a single molecule was extracted to yield a refined molecular model suitable for further calculations.

ZINDO, an INDO/1 SCF CI semi-empirical molecular orbital program that is parametrized for electronic spectroscopy of organic molecules, was written[36–38] and provided by Professor Michael Zerner of the University of Florida Quantum Theory Project, Gainesville, Florida. ZINDO was installed and operated on a CRAY Research Corporation C-90 supercomputer under UNICOS 8.0.2.2, at the San Diego Supercomputer Center, San Diego, California.

## Results and discussion

### Calorimetry

When a small sample of orange pendimethalin I is heated in a differential scanning calorimeter, three transitions are apparent in the thermogram, as shown in Fig. 2. The first transition, an endotherm, is followed by an exotherm (note that the valley between the peaks is below the baseline) and a second endotherm. These thermal events correspond to the melting of pendimethalin I at ~55 °C, recrystallization of the melt to form crystalline pendimethalin II, and the melting of pendimethalin II at ~57 °C, respectively. A sample of pure pendimethalin II, treated in the same way, exhibits only the higher temperature endotherm (data not shown). Note that the experimental thermogram includes a thermal lag of ~0.5 °C, which should be subtracted from the temperature axis to derive actual temperatures. Thus, differential scanning calorimetry unequivocally demonstrates the polymorphism of pendimethalin.

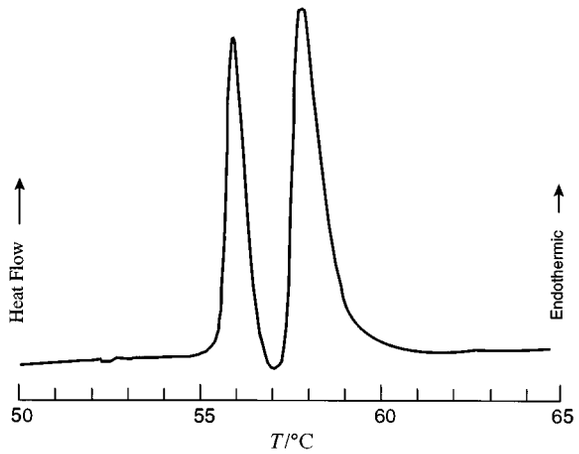


**Fig. 2** Differential scanning calorimetry of orange pendimethalin I. The thermal events correspond to melting of pendimethalin I at ~55 °C (endotherm), recrystallization of the melt to form crystalline pendimethalin II (exotherm), and melting of pendimethlin II at ~57 °C (endotherm). Note the instrument's thermal lag of ~0.5 °C.

### X-Ray structure

Single crystal X-ray diffraction patterns were collected for both pendimethalin polymorphs and a total of 2685 unique reflections, for $2 < \theta < 25°$ and $+h \pm k \pm l$, were gathered from an orange pendimethalin I crystal of dimensions 0.4 × 0.3 × 0.15 mm, and 1686 unique reflections with $|F^2| > \sigma(F^2)$ were used in the refinement. A total of 2964 reflections were gathered from a yellow pendimethalin II crystal of dimensions 0.35 × 0.20 × 0.08 mm, and 930 unique reflections with $|F^2| > \sigma(F^2)$ were used in the refinement. Note that $\sigma(F^2) = \{\sigma^2(I) + (0.04I)^2\}^{1/2}/L_p$. There was no crystal decay and no absorption correction was applied. The structures were solved by direct methods using the MULTAN computer program and refined by full matrix least squares with anisotropic temperature factors for the heavy atoms (C, N and O). The hydrogen atoms were located on a difference map and included in the refinement with isotropic temperature factors. The weighting scheme was $w = 1/\sigma^2(F)$ and the final residuals were R = 0.082, $R_w = 0.083$ for orange pendimethalin, and $R = 0.045$, $R_w = 0.056$ for yellow pendimethalin. The final difference maps were featureless.

The X-ray structures for the orange and yellow forms are illustrated in Fig. 3.† Orange pendimethalin (I) conforms to a triclinic space group ($P\bar{1}$) with unit cell dimensions: $a = 7.267(1)$ Å, $b = 9.526(2)$ Å, $c = 10.612(2)$ Å, $\alpha = 98.62(2)°$, $\beta = 90.20(1)°$, $\gamma = 106.38(1)°$. In contrast, yellow pendimethalin (II) exhibits a monoclinic space group ($P2_1/c$) with the unit cell dimensions: $a = 7.197(2)$ Å, $b = 21.973(4)$ Å, $c = 9.432(3)$ Å, $\alpha = 90.00°$, $\beta = 102.69(2)°$, $\gamma = 90.00°$. Yellow pendimethalin (II) has about twice the volume ($U$) and twice the number of molecules ($Z$) per unit cell of the orange I form. The calculated density is 1.28 g cm$^{-3}$ for both forms. The unit cells ($bc$ face projections) are illustrated in Fig. 4.

In the unit cell, both crystal habits of pendimethalin involve parallel stacking of aromatic rings. As shown in Fig. 4, the molecules are oriented 180° out of phase with molecules above and below in the same stack. Several experimental values for angles and torsions that differ significantly between the two polymorphs are given in Table 1. Most other angles, $\theta$, and torsions, $\varphi$, differ by less than 2°.

The structural differences between the orange and yellow

† Full crystallographic details, excluding structure factor tables, have been deposited at the Cambridge Crystallographic Data Centre (CCDC). For details of the deposition scheme, see 'Instructions for Authors', *J. Chem. Soc., Perkin Trans. 2*, available *via* the RSC Web page (http://www.rsc.org/authors). Any request to the CCDC for this material should quote the full literature citation and the reference number 188/138.

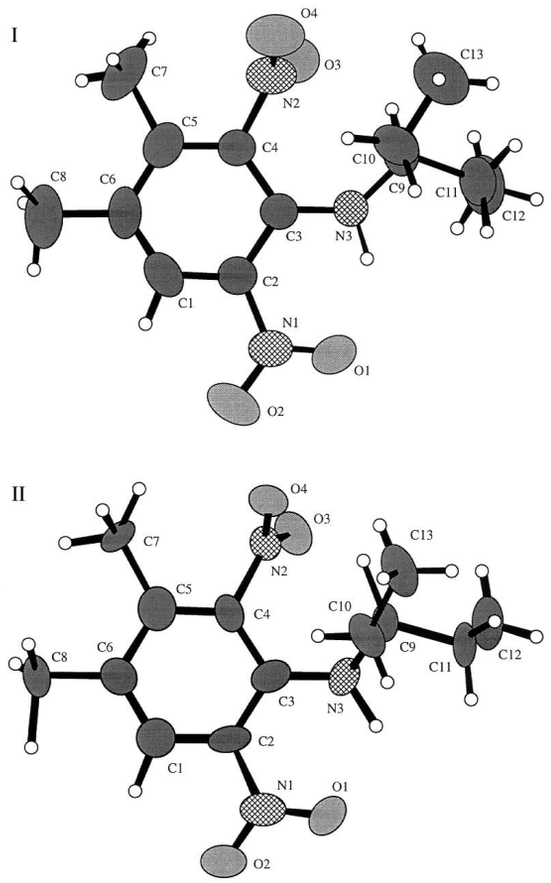


**Fig. 3** X-Ray diffraction structures of orange (I) and yellow (II) pendimethalin

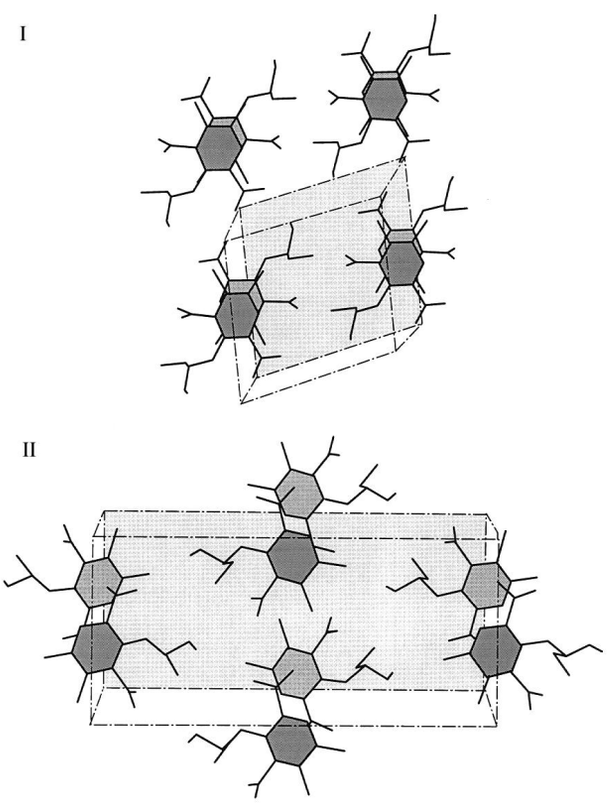


**Fig. 4** Unit cell geometry (*bc* face projections) for orange (I) and yellow (II) pendimethalin

forms are subtle. In both forms, the plane of the nitro group attached to carbon C4 is highly twisted relative to that of the aromatic ring (76° and 67° twists in the orange and yellow forms, respectively), due to steric hindrance by the adjacent methyl group and the 1-ethylpropyl side chain atoms, and crystal packing forces. In contrast, the plane of the nitro group on carbon C2 is only slightly twisted (*ca.* 10° in both forms), permitting one oxygen atom to participate in a hydrogen bond with the secondary amino hydrogen. The torsion $\varphi_2$ about the bond between the aromatic ring and the amino moiety, formed by atoms C9–N3–C3–C2, is 155.1° in the orange form and 141.0° in the yellow form, a 14° difference that may also be important in establishing the strength of the intramolecular hydrogen bond. This is the largest torsion difference between the polymorphs.

**Table 1** Bond angles ($\theta$) and torsions ($\varphi$) that differ significantly in orange and yellow pendimethalin

| Angle $\theta$ or torsion $\varphi$ | Atoms involved | Orange polymorph | Yellow polymorph |
|---|---|---|---|
| $\theta_1$ | N3–H–O1 | 143.0° | 118.5° |
| $\theta_2$ | N1–O1 ··· H–N3 | 102.0° | 113.0° |
| $\varphi_1$ | N1–O1 ··· H–N3 | −16.2° | −2.7° |
| $\varphi_2$ | C9–N3–C3–C2 | −155.1° | −141.0° |
| $\varphi_3$ | N3–C9–C11–C12 | 62.0° | 72.0° |
| $\varphi_4$ | N3–C9–C10–C13 | −170.4 | −168.7 |
| $\varphi_5$ | O1–N1–C2–C3 | −10.5° | −9.4° |
| $\varphi_6$ | O4–N2–C4–C3 | 75.6° | 66.9° |

As shown in Table 1, the torsions in the 'legs' of the chain, $\varphi_3$ (N3–C9–C11–C12) and $\varphi_4$ (N3–C9–C10–C13), differ by 10.0° and 1.7°, respectively, between the orange and yellow forms which results in a 5% shorter N3–C12 distance and smaller side-chain volume in the orange polymorph (see Fig. 3). This difference, although small, permits more overlap of adjacent aromatic rings in the orange form when viewed from the *bc* face. The two crystal forms have the same calculated density because the average spacing of molecules in all three dimensions is the same.

### Crystal structure refinement

We have attempted to use molecular modeling and quantum chemistry methods to account for the known properties of pendimethalin, especially the thermodynamic properties and spectra that distinguish the polymorphs. In the literature, there is a paucity of molecular modeling applications to the solid state, and especially to the prediction of crystal polymorphism. Notable in the literature is the pioneering work of Hagler and Bernstein, who demonstrated that crystal packing is dominated by van der Waals forces,[39,40] except in crystals where strong intermolecular hydrogen bonding prevails.[41] The atomic coordinates derived from X-ray diffraction represent centers of maximum electron density rather than true nuclear coordinates, making the X-ray structure unsuitable for the calculation of molecular orbitals and electronic transition energies. Most prominently, the carbon hydrogen bond lengths are too short by about 10%, and the calculated potential energy of the X-ray structure is too high by *ca.* 200 kcal mol$^{-1}$. The use of molecular mechanics or quantum mechanics to optimize the geometry of a single molecule, unrestrained by a lattice, results in a 'gas phase' minimum energy structure that does not resemble the molecule in either crystal habit, due to 'free' rotations about single bonds. What is needed is a strategy for geometry optimization in the crystal field.

As discussed by Warshel and Lifson,[42] crystal packing is determined by a large number of small forces that yield a broad minimum in the potential energy well. van der Waals forces, which make the greatest contribution to the lattice energy and are important in determining unit cell dimensions, act over distances greater than 10 Å. The lattice energy of the polymorphic crystals of pendimethalin were calculated using two different approaches, as described in the Experimental section. The 'central molecule in a rigid lattice' approach was used to iteratively

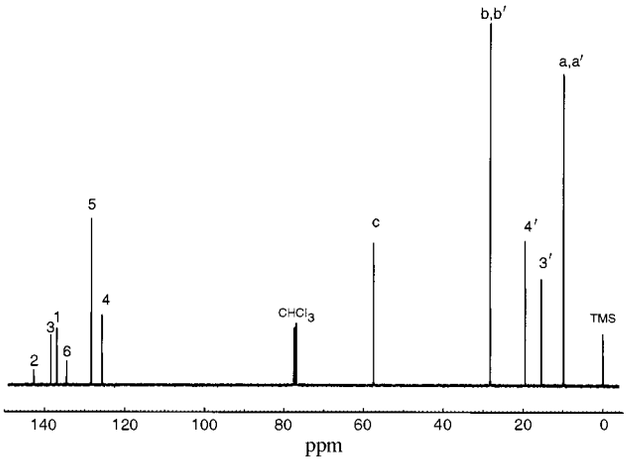


**Fig. 5** Carbon-13 NMR spectrum of pendimethalin in chloroform solution

refine the structure, taking into account non-bonded interactions at distances up to 15 Å. In the second approach, the molecular structures were optimized by minimization of a periodic lattice under periodic boundary conditions.

The two different computational methods for optimizing the geometry of pendimethalin molecules in the crystal lattice yielded estimates of the lattice energy which suggest that the orange form of pendimethalin is stabilized by *ca.* 4 to 5 kcal $mol^{-1}$ relative to the yellow form. This is a reasonable estimate consistent with the known stabilities of the polymorphs. Note that the lattice energies reported here correspond to the calculated heats of sublimation at a temperature of zero degrees Kelvin. While it is unrealistic to expect that energies calculated in this way will reproduce the experimental lattice energies, if these are known, it is conventionally argued that the calculation errors are systematic and that differences in calculated lattice energies for similar molecules are meaningful. Improved computational approaches for the solid state are being developed[11,43,44] and a force field that is parametrized for organic molecules in crystals has been described recently.[45]

## Carbon 13 NMR

The $^{13}C$ NMR spectrum of pendimethalin in a chloroform solution is shown in Fig. 5. The aliphatic resonances of the $^{13}C$ solid state CP-MAS NMR spectra of the orange and yellow forms of pendimethalin, respectively, are shown in Fig. 6. Similarly, Fig. 7 shows the aromatic resonances. The $^{13}C$ chemical shift assignments are listed in Table 2 (with respect to the atomic numbering shown in Fig. 1) for pendimethalin in chloroform solution and for the orange and yellow forms in the polycrystalline state. The assignment for the protonated aromatic carbon C-5 in the CP-MAS spectrum was unambiguously determined by an independent separated local field experiment.[46] All other aromatic assignments in the solid state were made by analogy with the definitively assigned solution spectrum, for which short and long range CH couplings and single frequency decoupling data were generated.

The nuclear shielding differences, $\Delta\delta$, between the orange and yellow forms are also listed in Table 2. Fig. 8 shows a spectrum of a sample containing a mixture of the orange and yellow polymorphs. The near baseline resolution of the 4′ methyl group resonances at *ca.* 20 ppm implies a possible method for quantitative measurement of the orange and yellow polymorph in mixtures of the two.

Previously reported NMR studies have shown that the combined cross polarization[47] and magic angle spinning technique[48,49] is capable of distinguishing crystal polymorphs.[50,51] Similarly, several $^{13}C$ resonances in pendimethalin are distinguishable in the orange and yellow polymorphs. It is obvious from the shielding differences, $\Delta\delta$, listed in Table 2 that all

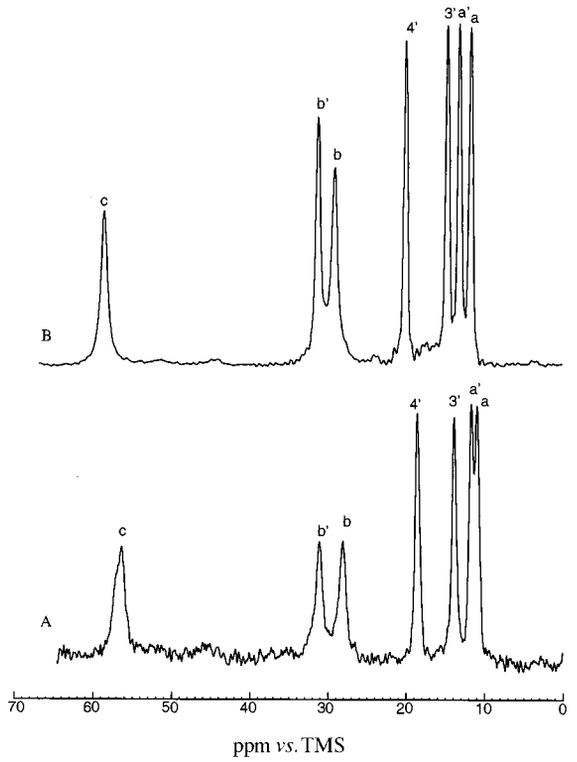


**Fig. 6** Carbon-13 CP-MAS NMR spectra of (A) orange (I) and (B) yellow (II) pendimethalin showing the aliphatic resonances

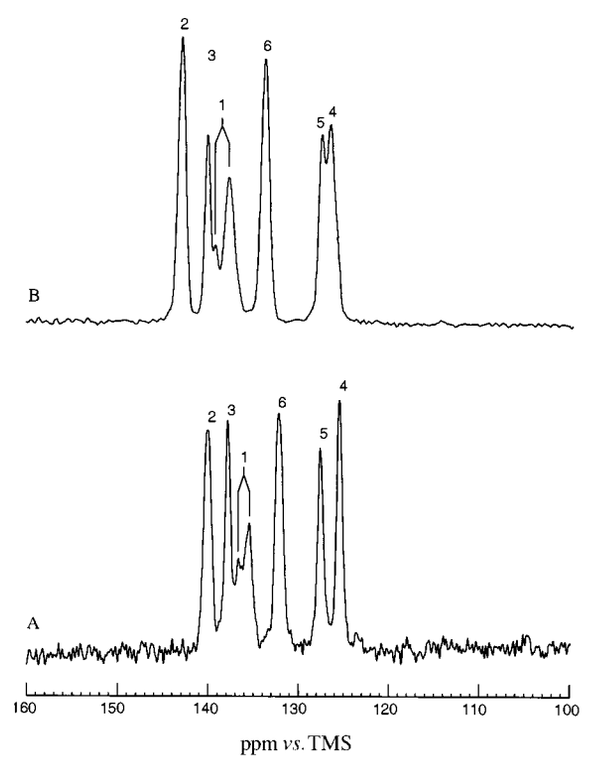


**Fig. 7** Carbon-13 CP-MAS NMR spectra of (A) orange (I) and (B) yellow (II) pendimethalin showing the aromatic resonances. The splitting of C-1 resonance by the $^{14}N$ of the amino group is notable.

resonances except that of C-5 are deshielded in the yellow form relative to the orange polymorph. Examination of these differences reveals that they are largest for carbons closest to the secondary amino group. The shieldings in pendimethalin crystals are derived from a combination of intra- and intermolecular electronic effects. The parallel stacking of aromatic rings in adjacent rows must generate a ring current effect on

**Table 2** Carbon-13 NMR chemical shift assignments for pendimethalin in chloroform solution and its crystal polymorphs I and II in the solid state

| Carbon number | Chloroform solution $\delta$ (ppm) | Orange solid (I) $\delta$ (ppm) | Yellow solid (II) $\delta$ (ppm) | Yellow–orange difference $\delta$ (ppm) |
|---|---|---|---|---|
| 1 | 136.93 | 136.0* | 138.5 | 2.5 |
| 2 | 142.61 | 140.1 | 142.8 | 2.7 |
| 3 | 138.39 | 137.8 | 139.9 | 2.1 |
| 4 | 125.68 | 125.4 | 126.3 | 0.9 |
| 5 | 128.37 | 127.6 | 127.2 | −0.4 |
| 6 | 134.43 | 132.9 | 133.6 | 0.5 |
| 3′ | 15.37 | 13.9 | 14.6 | 0.7 |
| 4′ | 19.38 | 18.5 | 20.0 | 1.5 |
| a | 9.82 | 10.9 | 11.7 | 0.8 |
| a′ | 9.82 | 11.7 | 13.2 | 1.5 |
| b | 28.16 | 28.0 | 29.1 | 1.1 |
| b′ | 28.16 | 31.1 | 31.2 | 0.1 |
| c | 57.43 | 56.4 | 58.5 | 2.1 |

* Broad doublet due to residual $^{14}N$–$^{13}C$ coupling.

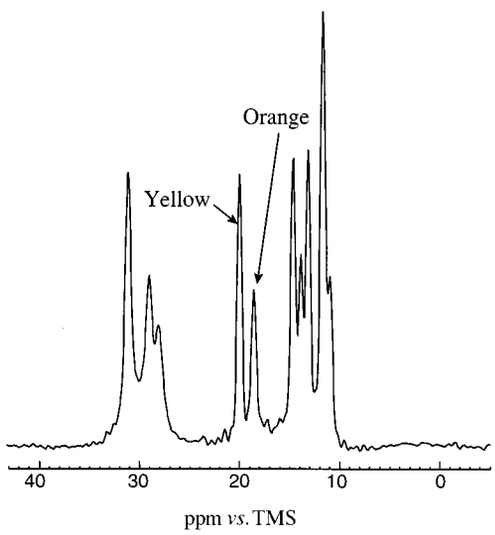


**Fig. 8** Carbon-13 CP-MAS NMR spectrum of a mixture of orange (I) and yellow (II) pendimethalin showing the distinguishing aliphatic resonances useful for quantitative analysis

neighboring molecules. However, this effect is expected to be small due to the large distances (>7 Å) involved. The largest effect is most likely to be the delocalization of the amino nitrogen lone pair into the aromatic π-electron system, as discussed in more detail below.

In the CP-MAS spectra, the resonances for one aromatic and one aliphatic carbon show an interesting splitting. As described by Hexam *et al.*,[52] resonances of carbons bonded to nitrogen are broadened and often split into asymmetric doublets when all other carbons are narrow singlets, due to the fact that MAS does not completely average the $^{14}N$–$^{13}C$ dipolar interaction because the large $^{14}N$ quadrupole interaction tilts the quantization axis of the $^{14}N$ spins away from the direction of the applied field. The resonances exhibiting this phenomenon have been assigned to aromatic carbon C-1 and the methine carbon C-C, which are both bonded to the secondary amino nitrogen. The aromatic carbons connected to the nitro groups do not show significant splittings.

The near baseline resolution of the 4′ methyl group resonances at *ca.* 20 ppm in a mixture of orange and yellow polymorphs, as shown in Fig. 8, provides an extremely useful method of quantitative analysis. Indeed, the presence of as little as 2% orange polymorph in samples of predominantly yellow pendimethalin, or vice versa, can be determined in both technical and formulated materials. In our laboratory, $^{13}C$ CP-MAS

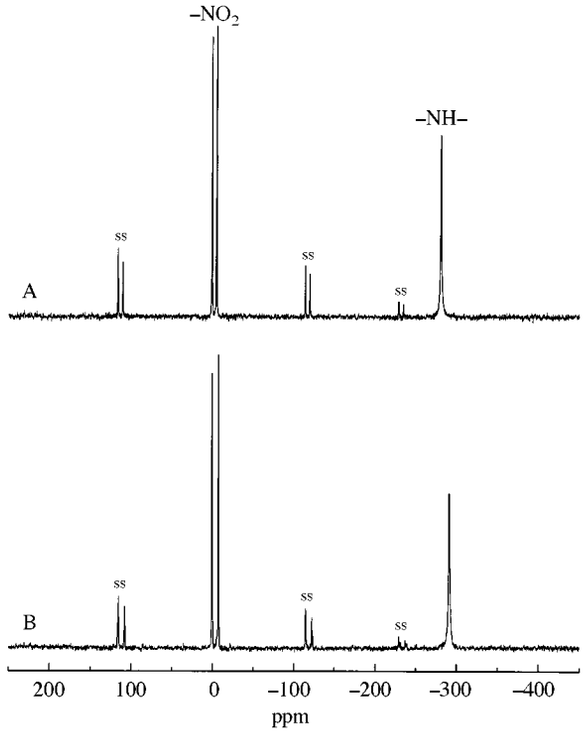


**Fig. 9** Nitrogen-15 CP-MAS NMR spectra of (A) orange (I) and (B) yellow (II) pendimethalin

NMR has been used routinely during the past decade to track the polymorphic composition of such materials, and to monitor the yellow to orange phase transition over time.

### Nitrogen 15 NMR

The solid state $^{15}N$ NMR spectra of the yellow and orange polymorphs of pendimethalin are shown in Fig. 9. The nitrogen of the 2-position nitro group resonates at −0.144 and −0.151 ppm in the orange and yellow forms, respectively, whereas the nitro group on carbon 6 (N-6′) is deshielded to −5.5 and −8.0 ppm in the orange and yellow forms. In contrast, the amino nitrogen resonates at −281.967 and −292.043 ppm in the orange and yellow forms ($^{15}N$ chemical shifts are referenced to $^{15}NO_3$ in ammonium nitrate).

The observation that the nitrogen of the 2-position nitro group resonates very near 0 ppm (in both polymorphs) suggests that this nitro is not involved in hydrogen bonding. In contrast, the significant upfield shift ($\Delta\delta = -5.5$ and −8.0 ppm) of the 6-position nitro group suggests the formation of a strong hydrogen bond, most probably an internal one to the secondary amino hydrogen, which will increase electron density at the amino nitrogen and thus shield this nucleus. Moreover, the $^{15}N$ spectra show that the hydrogen bond is present in both forms of pendimethalin. While the amino nitrogen resonances are very well resolved in the two polymorphs, $^{15}N$ NMR has insufficient sensitivity for routine analytical applications and $^{13}C$ CP-MAS NMR has proven to be more useful for quantitative analysis.

### Proton NMR

The proton spectra of solid pendimethalin (Fig. 10) were obtained using CRAMPS (combined rotation and multiple pulse spectroscopy) experiments.[31] The single aromatic proton at position 5 resonates at 6.8 and 7.4 ppm in the yellow (II) and orange (I) polymorphs, respectively. The secondary amino proton at position 1′ is more difficult to assign. By analogy to the solution spectra[53] of the non H-bonded amino protons of aniline at 3.35, and the H-bonded amino proton of *o*-nitroaniline which is deshielded at 6.2 ppm; the amino proton at position 5 in pendimethalin is assigned at 5.2 ppm in the yellow polymorph. However the amino proton of the orange (I)

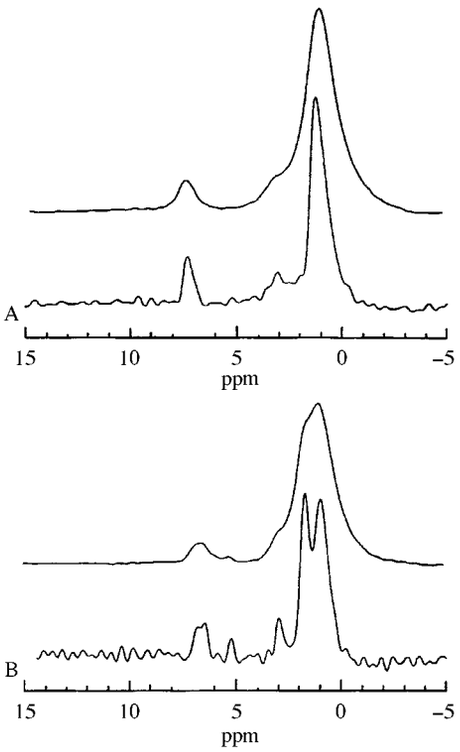


**Fig. 10** Solid state proton NMR spectra of (A) orange (I) and (B) yellow (II) pendimethalin *via* combined rotation and multiple pulse spectroscopy (CRAMPS)

polymorph at *ca.* 7 ppm is almost coincident with the aromatic proton and is less confidently assigned.

The above assignments suggest that the aromatic 5 proton is deshielded to low field by 0.6 ppm, and the secondary amino proton at position 1′ is deshielded to low field by *ca.* 1.8 ppm in the orange (I) polymorph compared to the yellow (II) polymorph. These observations indicate that the π-electron density in the yellow (II) polymorph is being delocalized further into the adjacent fused pseudo six-membered ring formed by the stronger hydrogen bond in the orange (I) polymorph.

### Infrared and resonance Raman spectra

Resonance Raman spectra in the region 1200–1400 $cm^{-1}$ are shown in Fig. 11, and the diffuse reflectance FT IR measurements are illustrated in Fig. 12. The interesting spectral features are listed in Table 3. Unequivocal assignments for the vibrational spectra are difficult since most bands are combination modes. However, bands near 3300, 1530, 1330, and 630 $cm^{-1}$, which arise from the N–H stretch, asymmetric and symmetric $NO_2$ stretching motions, and $NO_2$ out of plane bending, respectively, can be safely interpreted. In the resonance Raman spectra, the most striking differences between the yellow and orange forms lie in the nitro frequencies, which differ by ~11 $cm^{-1}$, and in the relative intensity of the combination band at 1245 $cm^{-1}$ in the yellow and 1234 $cm^{-1}$ in the orange form.

Infrared and Raman vibrational spectra are known to differentiate polymorphs, at least in favorable cases,[54] and both of these methods can provide evidence for hydrogen bonding. The N–H stretching mode in secondary aromatic amines usually appears near 3450 $cm^{-1}$ and this is not strongly affected by neighboring electron withdrawing groups unless they participate in a hydrogen bond to the amino hydrogen. The interesting features of the vibrational spectra of pendimethalin are listed in Table 3. In the DRIFT spectrum, the N–H stretch moves to 3326.5 $cm^{-1}$ in the yellow polymorph and to 3318.6 $cm^{-1}$ in the orange form, suggesting involvement of the N–H in a hydrogen bond, which may be slightly stronger in orange pendimethalin I. This observation is consistent with the shorter H-bond length inferred from the X-ray diffraction results. The $NO_2$ asymmetric stretch at 1532 $cm^{-1}$ is virtually the same in both forms, while the out-of-plane bend appears at 672.7 $cm^{-1}$ in the yellow polymorph and at 630.3 $cm^{-1}$ in the orange form.

In the resonance Raman spectra, the most striking differences between the yellow and orange forms lie in the nitro

**Table 3** Resonance Raman and infrared vibrational frequencies for pendimethalin. Bands designated 'Mixed Mode' are combination bands arising from C–C and C–N stretch and C–H in plane deformation

| Infrared $\tilde{\nu}/cm^{-1}$ | Orange (I) Raman $\tilde{\nu}/cm^{-1}$ | Yellow (II) infrared $\tilde{\nu}/cm^{-1}$ | Raman $\tilde{\nu}/cm^{-1}$ | Assignment |
|---|---|---|---|---|
| 3318.6 | | 3326.5 | | N–H-stretch |
| 1531.8 | | 1532.0 | | $NO_2$-asymmetric-stretch |
| 1330.1 | 1336 | 1321.6 | 1325 | $NO_2$-symmetric-stretch |
| | | | 1219 | Mixed-mode |
| | 1234 | | | |
| | | | 1245 | |
| | 1297 | | 1295 | |
| 630.3 | | 672.7 | | $NO_2$-out-of-plane-bend |

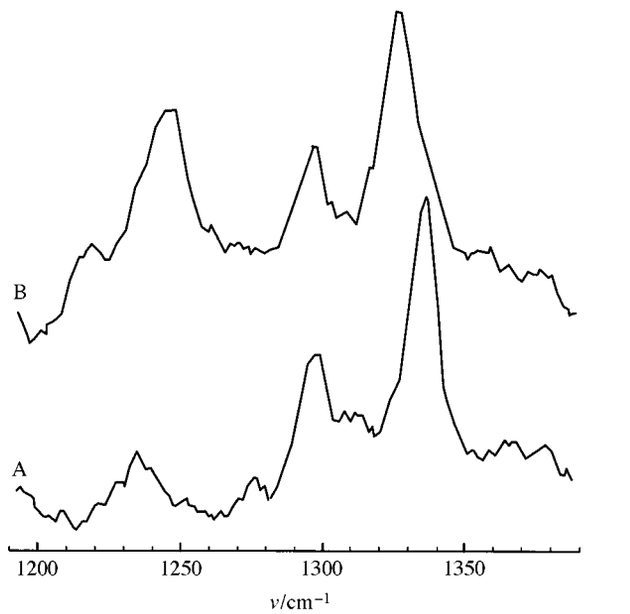


**Fig. 11** Resonance Raman spectra of (A) orange (I) and (B) yellow (II) pendimethalin

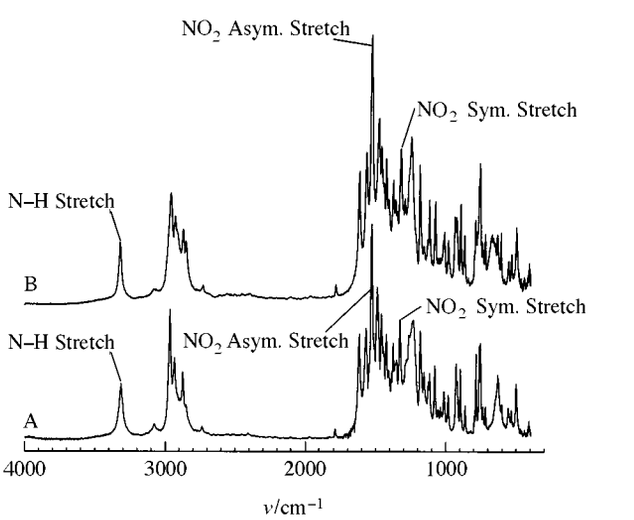


**Fig. 12** Diffuse reflectance Fourier transform infrared spectrum of (A) orange (I) and (B) yellow (II) pendimethalin

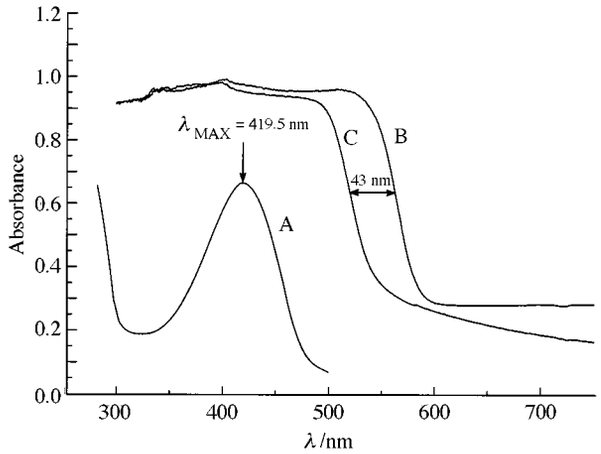


**Fig. 13** Diffuse reflectance UV–VIS spectra of pendimethalin: (A) $1 \times 10^{-4}$ M solution in hexane; (B) orange (I) crystals; (C) yellow (II) crystals

frequencies, which differ by ~11 $cm^{-1}$, and in the relative intensity of the combination band at 1245 $cm^{-1}$ in the yellow and 1234 $cm^{-1}$ in the orange form. The $NO_2$ symmetric stretch normally occurs near 1350 $cm^{-1}$ and moves to lower frequencies in the presence of neighboring electron withdrawing groups.[55] The higher frequency for the orange *vs.* yellow polymorph (1336 $cm^{-1}$ *vs.* 1325 $cm^{-1}$ in the Raman and 1330.8 $cm^{-1}$ *vs.* 1322.1 $cm^{-1}$ in the infrared) may result from three competing effects which are not easily quantified: (a) a hydrogen bond to the nitro group decreases electron density in the N O bond and hence, its stretching frequency (*i.e.* lower frequency implies a stronger hydrogen bond); (b) a stronger hydrogen bond to the nitro group will shift electron density to the amino nitrogen, increase the delocalization of the amino nitrogen lone pair into the ring, increase the double bond character of the C–$NO_2$ bonds, increase the electron density in the $NO_2$ groups, and increase the vibrational frequency; (c) a small contribution to the $NO_2$ symmetric stretch may occur from the mixing of other vibrational modes which may be different in the two polymorphs. However, it is likely that the first mechanism will produce the largest effect.

**Electronic spectra**

The electronic absorption spectra for pendimethalin in hexane solution and in the solid state are shown in Fig. 13. A $1 \times 10^{-4}$ M solution of pendimethalin in hexane is coloured yellow and exhibits a symmetrical long wavelength absorption band maximum at 419 nm with a half width at half height of 82 nm; the molar extinction coefficient $\lambda_{max} = 5201$.[56] The diffuse reflectance spectra of solid orange (I) and yellow (II) pendimethalin, measured in an integrating sphere, exhibit a broad flat absorption maximum with a cutoff at longer wavelengths than in the solution spectrum. The difference between the long wavelength cutoffs for the orange and yellow polymorphs is 43 nm, measured at the point of inflection.

The electronic absorption spectra for pendimethalin (Fig. 13) differ by *ca.* 43 nm, measured at the point of inflection, which corresponds to an energy difference of *ca.* 1.24 kJ $mol^{-1}$. The observed spectral differences may be accounted for, at least qualitatively, in terms of intramolecular effects attributable to increased conjugation in the orange (I) form relative to the yellow (II) polymorph. Moreover, this mechanism is supported by the solid state $^{13}C$ NMR results in which the aromatic carbons connected to the secondary amino substituent and the 2-position nitro group are more shielded in the orange form than in the yellow polymorph.

Both the visual colours and the solid state UV–VIS absorption spectra of the pendimethalin polymorphs show that the long wavelength transition is shifted to lower energy (a red shift) in the orange (I) form with respect to the yellow (II) form. The observed transition intensities are similar in the two forms. The assignment of the origin of the long wavelength transition in simple nitroanalines is still a matter for discussion,[57] and the difficulty is compounded in pendimethalin by the secondary amino function attached to the chromophore. It is important to note that π–π* transitions are polarized in the plane of the aromatic ring and that n–π* transitions are perpendicular to that plane. However, in view of the X-ray crystal structures reported above, it is possible that the long wavelength transition is a combination of these modes. The polarization with respect to the molecular coordinates is, therefore, not known.

Notwithstanding these arguments, two theoretical approaches have been applied in attempts to account for the observed spectra of the pendimethalin polymorphs, (a) an exciton theory, which considers only intermolecular interactions between electronic states on neighboring molecules, and (b) a molecular orbital theory, which includes only intramolecular effects.

Exciton theory[58] is a theory of delocalized electronic states that has been used to calculate electronic transitions in organic crystals. Förster[59] describes an 'electronic transannular' effect between adjacent molecules in a crystal caused by an exciton transition dipole coupling, which is an entirely intermolecular effect. The electronic Hamiltonian, $\hat{H}$, for a system of $N$ stationary molecules with fixed nuclear positions is given by eqn. (1), where $\hat{H}_n$ is the Hamiltonian for a single molecule and

$$\hat{H} = \Sigma \hat{H}_n + \Sigma\Sigma V_{mn} \quad (1)$$

$V_{mn}$ is the electronic interaction potential between neighboring molecules. Thus, in Förster's nomenclature, the pseudo coulombic interaction is given by the resonance integral $U_{mn}$ between configurations with m and n excited, eqn. (2), which approx-

$$U_{mn} = \langle \varphi'_m \varphi_n | V_{mn} | \varphi_m \varphi'_n \rangle \quad (2)$$

imates to eqn. (3), where $R$ is the separation between dipoles on

$$U_{mn} = D/[n^2 R_n^3] \quad (3)$$

adjacent molecules, and $n$ is the refractive index of the medium (assumed to be 1). The dipole strength, $D$, is related to the area under the absorption band and to the classical oscillator strength. Under the simplifying assumptions of Mason,[60] the dipole strength is given by eqn. (4) where $h$ is Planck's constant,

$$D = [3hc10^3 \log_e 10/(2\pi)^3 N] \int (\varepsilon/\nu)\, d\nu = 91.8 \times 10^{40}\, \varepsilon \Delta\nu_{1/2}/\Delta\nu \quad (4)$$

$c$ the velocity of light, $\Delta\nu$ the transition frequency, $\Delta\nu_{1/2}$ the transition width at half height, and $\varepsilon$ the molar extinction coefficient.

Thus, the exciton effect is proportional to the intensity of the transition dipoles, inversely proportional to the cube of their separation, and is a function of their respective vector geometries. It causes a splitting of an absorption band into two components (the 'exciton splitting'). If the spectral shift was due to an intermolecular exciton interaction only, then Förster's model predicts that the interaction is due to approximately colinear 'head to tail' transition dipoles on adjacent molecules. Any other vector relationship between the dipoles would not be consistent with the observed spectra.

Fig. 4 shows that there are differences in the separation of molecules in adjacent molecular stacks between the two polymorphs. In the orange (I) form, this separation is about 9.5 Å, whereas in the yellow (II), form it is about 12 Å. Considering the possibility that the 'in plane' molecular transition dipoles on molecules in adjacent stacks are 'head-to-head' in the yellow

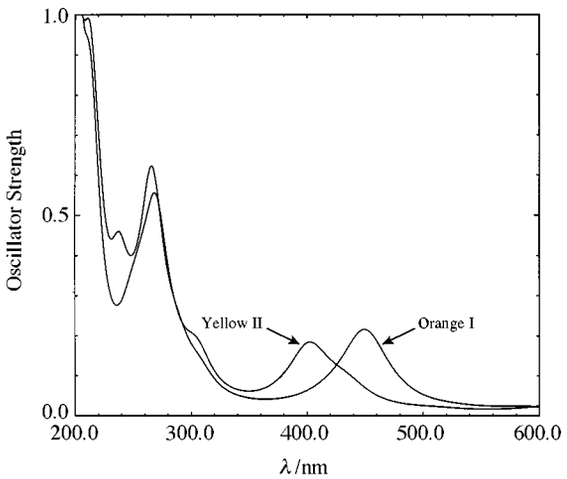


**Fig. 14** Simulated UV–VIS spectra of pendimethalin polymorphs. Spectra of single molecules with crystal geometries calculated by semi-empirical molecular orbital methods (INDO/1 with configuration interaction).

(II) polymorph (causing a blue shifted band of theoretically zero intensity), and are 'head-to-tail' in the orange (I) form (leading to a red shifted band of increased intensity), then a first approximation of the magnitude of the spectral shifts can be calculated from Förster's model. For simplicity, only the coulombic interaction between pairwise sums of 'head-to-tail' transition dipoles are considered and the transition charge densities are approximated to a point multipole series.[61] The electronic absorption process gives rise to an electric dipole transition moment which is related to the dipole strength. If two adjacent molecules are simultaneously excited, then the mixing of the two excited electronic configurations gives rise to a pseudo coulombic interaction which is proportional to both the dipole strength and the inverse cube of their separation. The latter geometrical requirement is significant. The calculated result is that the orange (I) form would show a red shift in the long wavelength absorption band of $U_{mn} \approx 57$ cm$^{-1} \approx 1$ nm, which is very small compared to the observed shift. Thus, the maximum possible exciton effect calculated in this way does not explain the observed spectral shift of 43 nm between the polymorphs. Although there are some differences in the positions of adjacent molecules within a crystallographic stack, they appear to be insignificantly small in this context. Transitions which cause molecular polarizations perpendicular to the aromatic rings do not appear to meet the geometrical requirements of Förster's model, and also do not explain the observed spectral shift between the polymorphs.

In a molecular orbital approach, the spectral transitions were computed entirely in terms of intramolecular contributions, in contrast to Förster's model. The molecular orbitals of a single pendimethalin molecule in each crystal geometry were calculated with the INDO/1 SCF CI semi-empirical molecular orbital approach using the computer program ZINDO, which is parametrized for accurate prediction of electronic transitions of organic molecules in dilute solution. The maximum configuration interaction (CI) permitted by the program's dimensions was used. For pendimethalin, which has 39 atoms, a maximum of 197 configurations is permitted. As shown in Fig. 14, the spectral shift in the longest wavelength transition between the orange and yellow forms of pendimethalin was found by this method to be 45 nm, which compares very favorably with the observed shift of 43 nm. Thus, it appears that the entire spectral shift can be accounted for in terms of transitions between molecular orbitals located on a single molecule, and that intermolecular contributions (*e.g.* charge transfer interactions) to the transition energies are negligible. In a different sense, the long wavelength transition is affected by interaction of a molecule with its neighbors in the crystal lattice since this interaction controls the molecular geometry and molecular orbital energies.

**The intramolecular hydrogen bond**

Although X-ray diffraction data do not locate the positions of hydrogen atoms with great accuracy, the best fit of the structural model to the electron density does suggest that the N–H···O hydrogen bond length is 1.90 Å in yellow pendimethalin, whereas it appears to be somewhat shorter at 1.83 Å in the orange form. This may result from the 14.1° difference in the four bond torsional angle $\varphi_2$ for the C9–N3–C3–C2 system. If the pseudo six-membered ring involving the hydrogen bond were planar, then all of the internal angles would be close to 120° and the torsion $\varphi_2$ would be 180°, rather than the observed values of $\varphi_2 = -155°$ and $-141°$ for orange and yellow pendimethalin, respectively. Thus, due to rotations about the C3–N3 bond of 30–40° and about the C2–N1 bond of ~10°, the pseudo ring is not planar and significant deviations in the bond angles from 120° occur, as shown in Table 1.

The requirements for a strong hydrogen bond to oxygen have been discussed in the literature, with little agreement between authors. In one of the earliest theories, the 'bent-bond' model of Bernal and Fowler,[62] and Pople,[63] the N–$\hat{H}$···O angle, $\theta$, the H-bond is viewed as 'straight' when $\theta = 180°$, and 'bent' when $\theta = 0°$. A bent bond is viewed as weaker than a straight hydrogen bond. However, according to Schneider's model for the hydrogen bond,[64] a stronger H-bond should manifest when its direction (N–H$\overrightarrow{\cdots}$O) is co-linear with the principal axis of the oxygen lone pair orbital (H···$\hat{O}$–N ~ 120°). Moreover, the van Duijneveldts[65] have argued, based on their molecular orbital calculations, that hydrogen bonds to oxygen become weaker and longer as the s-orbital character of the oxygen lone-pair increases, and that the bond strength is only weakly dependent on the H-bond angle.

Since the N–$\hat{H}$···O angle is 118.5° in the yellow (II) form and 143.8° in the orange (I) form, these three atoms are more co-linear in the orange polymorph and imply, in the bent-bond model, that the hydrogen bond in the orange (I) form is stronger. The H···$\hat{O}$–N angle is 101.65° in the orange I form and 112.96° in the yellow II form, which according to Schneider's argument would favor stronger hydrogen bond formation in the yellow form. However, the X-ray diffraction and spectroscopic evidence suggest that the hydrogen bond in pendimethalin I is stronger, shorter, and less bent than in pendimethalin II.

The solid state $^{13}$C, $^{1}$H and $^{15}$N chemical shift data support these notions of hydrogen bonding. The greater shielding of all aromatic carbons except those *meta* to the amino substituent in the orange form suggest increased delocalization of the amino lone pair into the aromatic π-orbital system in the orange form relative to the yellow form, which implies a stronger hydrogen bond in the orange polymorph. Similarly, the $^{15}$N results show an increased shielding for the amino nitrogen in the orange form, presumably due to transfer of electron density from the adjacent nitro group, *via* the H-bond, to the amino nitrogen. In the $^{1}$H NMR CRAMPS spectra, both the aromatic proton and the secondary amino proton are deshielded in the orange (I) form relative to the yellow (II) form by the same mechanism. This mechanism is also supported by the infrared and Raman frequencies, as discussed above.

**Quantitative analysis**

The various methods discussed in this report were evaluated as potential analytical tools for the quantitative measurement of polymorphs in technical grade pendimethalin and its formulations, which often contain both crystal forms simultaneously. The crystal habit in formulations is not readily characterized by inspection of colour since this is usually masked by coloured excipients. Reflectance spectrophotometry in the visible range is not useful for analysis as it is quite sensitive to particle size

as well as crystal habit. While calorimetry and the vibrational and electronic spectra also show clear differences for the two polymorphs of pendimethalin in pure form, their resolution is insufficient to identify or quantify a small amount of one form in the presence of the other. They also have the disadvantage that substantial energy is transferred to the specimen, causing heating and possibly disturbing the phase equilibrium (calorimetry is by nature destructive to the specimen). For practical analytical purposes, $^{13}$C CP-MAS NMR provides the most sensitive and definitive evidence of the transition from the yellow to the orange form, and is the least invasive of the instrumental methods. This technique is generally unencumbered by background interferences and it provides an ability to determine as little as 2% of orange pendimethalin in a sample of predominantly yellow polymorph (see Fig. 8). Nevertheless, there have been very few literature reports of NMR studies of polymorphism.[3,66] CP-MAS $^{13}$C NMR has been used extensively by us to track changes in polymorphic composition of candidate formulations of pendimethalin for potential use in agriculture. Many solid formulations, including wettable powders containing a predominance of clays, silica or alumina, solid-in-liquid suspensions (suspensible concentrates), and even polymer microcapsules, have been successfully characterized by CP-MAS $^{13}$C NMR.

## Conclusions

A combination of calorimetry, single-crystal X-ray diffraction, solid-state NMR, resonance Raman and infrared spectroscopy, UV–VIS spectroscopy and theoretical methods were used to characterize the two known crystal habits of pendimethalin, a dinitroaniline herbicide. All of these methods are capable of distinguishing different crystal forms. However, CP-MAS $^{13}$C NMR is the method of choice for the quantitative analysis of mixtures of the yellow and orange polymorphs since less than 2% yellow polymorph in a predominantly orange pendimethalin sample can be detected by this method. The technique is applicable to both solid formulations (*e.g.* wettable powders) and solid-in-liquid suspensions (suspensible concentrates). However, detailed structural information on the two polymorphs was obtained only by recourse to X-ray crystallographic methods. The driving force for the yellow (II) to orange (I) polymorphic transition is attributed to the change in the electronic delocalization achieved from shortening, strengthening, and partially straightening the 'bent' hydrogen bond between the secondary amino hydrogen and an oxygen of the 6′-nitro group. This results in increased overlap between the amino nitrogen's lone pair and the π-electron orbitals of the aromatic ring. The calculated lattice stabilization energy due to this process is 4 to 5 kcal mol$^{-1}$, and the calculated lattice energies are consistent with the observed stabilities of the polymorphs. The slow kinetics of this polymorphic transition are largely governed by the steric interaction of the 1-ethylpropyl side chain and the two nitro groups during crystallization, the more compact side-chain molecular conformation required for the energetically more stable orange (I) polymorph to form being more difficult to achieve than that required for the yellow (II) polymorph. The colour change from yellow to orange during the polymorphic transition is attributed to intramolecular electronic effects (increased delocalization of the secondary amino nitrogen lone-pair electrons into the aromatic ring and nitro groups), rather than to differences in the intermolecular exciton.

## Acknowledgements

The authors gratefully acknowledge Dr Edward Donoghue and Mr Edward Mikalsen of American Cyanamid Company, Dr Anthony Bielecki of Bruker Instruments, Dr Barry J. Say of the University of Durham, Industrial Research Laboratories, Dr Michael Lawless of Tripos Associates Inc, and Dr Michael Stapleton of Molecular Simulations Inc for their expert assistance in generating some of the results presented in this paper. We are also obliged to Dr Karl-Heinz Ott of American Cyanamid for his careful reading of the manuscript and for many helpful suggestions.

## References

1 G. R. Desiraju, *Science*, 1997, **278**, 404.
2 A. S. Meyerson, *Handbook of Industrial Crystallization*, Butterworth–Heinemann Series in Chemical Engineering, ed. H. Brenner, Butterworth–Heinemann, Boston, 1993.
3 T. L. Threlfall, *Analyst*, 1995, **120**, 2435.
4 G. Clydesdale, K. J. Roberts and R. Docherty, *J. Cryst. Growth*, 1994, **135**, 331.
5 G. Clydesdale, K. J. Roberts, K. Lewtas and R. Docherty, *J. Cryst. Growth*, 1994, **141**, 443.
6 R. J. Davey, *J. Cryst. Growth*, 1975, **29**, 212.
7 R. J. Davey, *J. Cryst. Growth*, 1976, **34**, 109.
8 Z. Berkovitch-Yellin, *J. Am. Chem. Soc.*, 1985, **107**, 3111.
9 Y. Weisinger-Lewiz, F. Frolow, R. K. McMullan, T. F. Koetzle, M. Lahav and L. Leiserowitz, *J. Am. Chem. Soc.*, 1989, **111**, 1035.
10 H. W. Karfunkel, F. J. J. Leusen and R. J. Gdanitz, *J. Comput.-Aided Mater. Des.*, 1993, **1**, 177.
11 K. T. Thomson, R. M. Wentzcovitch and M. S. T. Bukowinski, *Science*, 1996, **274**, 1880.
12 G. Clydesdale, K. J. Roberts and R. Docherty, *J. Cryst. Growth*, 1996, **166**, 78.
13 R. Docherty, G. Clydesdale, K. J. Roberts and P. Bennema, *J. Phys. D: Appl. Phys.*, 1991, **24**, 88.
14 M. H. J. Hottehuis, J. G. E. Gardeniers, L. Jetten and P. Bennema, *J. Cryst. Growth*, 1988, **92**, 171.
15 P. Hartman and P. Bennema, *J. Cryst. Growth*, 1980, **49**, 145.
16 P. Hartman, *J. Cryst. Growth*, 1980, **49**, 157.
17 J. D. H. Donnay and D. Harker, *Am. Mineral.*, 1937, **22**, 446.
18 W. T. M. Mooij, B. O. van Eijck, S. L. Price, P. Verwer and J. Kroon, *J. Comput. Chem.*, 1998, **19**, 459.
19 A. Gavezotti, *Acc. Chem. Res.*, 1994, **27**, 309.
20 A. Gavezotti, *Curr. Opin. Solid State Mater. Sci.*, 1996, **1**, 501.
21 G. Clydesdale and K. J. Roberts, *Langmuir*, 1996, **12**, 5722.
22 P. L. Sprankle, *Proc. Br. Weed Control Conf.*, *12th*, 1974, **2**, 825.
23 *The Pesticide Manual incorporating the Agrochemicals Handbook*, British Crop Protection Council, Surrey, UK, and The Royal Society of Chemistry, London, UK, 10th edn., 1994.
24 F. L. Ashton and A. S. Crofts, *Mode of Action of Herbicides.*, Wiley, New York, 1981.
25 *Solid/Liquid Dispersions*, ed. Th. F. Tadros, Academic Press, New York, 1987.
26 The work described in this paper aided the development of a physically stable suspension concentrate formulation for pendimethalin, as described by L. J. Morgan and M. Bell, US Patent No. 4 871 392, October 3, 1989, and L. J. Morgan, US Patent No. 4 875 929, October 24, 1989.
27 G. Germain, P. Main and M. M. Woolfson, *Acta Crystallogr.*, *Sect. B*, 1970, **26**, 91.
28 E. R. Andrew, A. Bradbury and R. G. Eades, *Nature*, 1958, **182**, 1659.
29 B. Schneider, D. Doskocilova, J. Babka and Z. Ruzicka, *J. Magn. Reson.*, 1980, **37**, 41.
30 W. T. Dixon, J. Schaefer, E. O. Stejskal and R. A. McKay, *J. Magn. Reson.*, 1982, **49**, 341.
31 G. Scheler, U. Haubenreisser and H. Rosenberger, *J. Magn. Reson.*, 1981, **44**, 134.
32 W. Kiefer and H. J. Bernstein, *Appl. Spectrosc.*, 1971, **25**, 609.
33 *SYBYL Molecular Modeling Software*, version 5.2 is a product of Tripos Associates, Inc, a Subsidiary of Evans and Sutherland, 1699 S. Hanley Rd., Suite 303, St. Louis, Missouri 63144.
34 *CERIUS Crystal Modeling Software*, Molecular Simulations Inc, Burlington, Massachusetts.
35 S. L. Mayo, W. A. Godard III and B. D. Olafson, *J. Phys. Chem.*, 1990, **94**, 8897.
36 J. E. Ridley and M. C. Zerner, *Theor. Chim. Acta.*, 1973, **32**, 111.
37 M. C. Zerner, G. H. Loew, R. F. Kirchner and U. T. Mueller-Westerhoff, *J. Am. Chem. Soc.*, 1980, **102**, 589.
38 W. D. Edwards, B. Weiner and M. C. Zerner, *J. Am. Chem. Soc.*, 1986, **108**, 2196.
39 J. Bernstein and A. T. Hagler, *J. Am. Chem. Soc.*, 1978, **100**, 673.
40 A. T. Hagler and J. Bernstein, *J. Am. Chem. Soc.*, 1978, **100**, 6349.
41 J. Bernstein, *Acta Crystallogr.*, *Sect. B*, 1979, **35**, 360.

42 A. Warshel and S. Lifson, *J. Chem. Phys.*, 1970, **53**, 582.
43 R. M. Wentzcovitch, *Phys. Rev. B: Condens. Matter*, 1991, **44**, 2358.
44 R. M. Wentzcovitch, J. L. Martins and G. D. Price, *Phys. Rev. Lett.*, 1993, **70**, 3947.
45 A. Gavezotti, *NATO ASI Ser.*, *Ser. C*, 1994, **426**, 51.
46 R. K. Hester, J. L. Ackerman, J. L. Neff and J. S. Waugh, *Phys. Rev. Lett.*, 1976, **36**, 1081.
47 A. Pines, M. G. Gibby and J. S. Waugh, *J. Chem. Phys.*, 1973, **59**, 569.
48 J. Schaefer and E. O. Stejskal, *J. Am. Chem. Soc.*, 1976, **98**, 1031.
49 C. A. Fife, *Solid State NMR for Chemists*, CFC Press, Guelf, Ontario, Canada, 1983.
50 J. A. Ripmeester, *Chem. Phys. Lett.*, 1980, 536.
51 C. Doherty and P. York, *Int. J. Pharm.*, 1988, **47**, 141.
52 J. G. Hexam, M. H. Frey and S. J. Opella, *J. Chem. Phys.*, 1982, **77**, 3847.
53 *The Aldrich Library of NMR Spectra*, Pouchert and Campbell, 1974.
54 J. C. Bellows and F. P. Chen, *Drug Dev. Ind. Pharm.*, 1977, **3**, 451.
55 K. Kumar and P. Carey, *J. Chem. Phys.*, 1975, **63**, 3697.
56 S. F. Mason, *Q. Rev. Chem. Soc.*, 1961, **15**, 287.
57 R. W. H. Berry, *Chem. Br.*, 1987, **23**, 210.
58 A. S. Davydov, *Theory of Molecular Excitons*, McGraw-Hill, New York, 1962.
59 *Light and Organic Crystals*, Th. Förster, in *Modern Quantum Chemistry*, ed. O. Sinanoglu, Academic Press, New York, 1965, pp. 93–137.
60 S. F. Mason, *Q. Rev. Chem. Soc.*, 1963, **17**, 20.
61 W. Kauzman, *Quantum Chemistry*, Academic Press, New York, 1957.
62 J. D. Bernal and R. H. Fowler, *J. Chem. Phys.*, 1933, **1**, 515.
63 J. A. Pople, *Proc. R. Soc. London*, *Ser. A*, 1951, **205**, 163.
64 W. G. Schneider, *J. Chem. Phys.*, 1955, **23**, 26.
65 J. C. M. van Duijneveldt-van de Rijdt and F. B. van Duijneveldt, *J. Am. Chem. Soc.*, 1971, **93**, 5644.
66 S. P. Srivastara, J. Handoo, K. M. Agrawal and G. C. Joshi, *J. Phys. Chem. Solids*, 1993, **54**, 639.

*Paper* 7/05178F
*Received* 18*th July* 1997
*Accepted* 10*th June* 1998